



MULTIFOCUS IMAGE FUSION BASED ON NONSUBSAMPLED CONTOURLET TRANSFORM AND SPIKING CORTICAL MODEL

Nianyi Wang*, Yide Ma[†], Weilan Wang*, Kun Zhan[†]

Abstract: A novel image fusion algorithm based on nonsubsampled contourlet transform (NSCT) and spiking cortical model (SCM) is proposed in this paper, aiming at solving the fusion problem of multifocus images. The fusion rules of subband coefficients of NSCT are discussed, and a new maximum selection rule (MSR) is defined to fuse low frequency coefficients instead of using traditional MSR directly. For the fusion rule of high frequency coefficients, spatial frequency (SF) of each high frequency subband is considered as the gradient features of images to motivate SCM networks and generate pulse of neurons, and then the time matrix of SCM is set as criteria to select coefficients of high frequency subband. Experimental results and visual evaluation demonstrate the effectiveness of the proposed fusion method. Objective tests and analysis conducted under different noised source image environments proved the robustness of the proposed fusion method.

Key words: *nonsubsampled contourlet transform (NSCT), spiking cortical model (SCM), multifocus image fusion, pulse coupled neural network (PCNN)*

Received: February 28, 2013

DOI: 10.14311/NNW.2015.25.031

Revised and accepted: March 30, 2015

1. Introduction

Image fusion integrates the complementary information from two or more images into a single composite image. The result provides a more informative and comprehensive description, and is more suitable for human visual perception. Fused image benefits the image analysis in many fields, such as in remote sensing, intelligent robot, machine vision, clinical medicine and molecular biology.

There are many kinds of image fusion methods. Along them, those methods that based on multiscale decomposition (MSD) of source images become more popular and important tools in recent years. MSD methods decompose source images into high frequency and low frequency subbands. Detailed and coarse features remain in the two types of subbands, respectively [28].

*Nianyi Wang – Corresponding author, Weilan Wang, School of Mathematics and Computer Science, Northwest University for Nationalities, China, Email: livingsailor@gmail.com

[†]Yide Ma, Kun Zhan, School of Information Science and Engineering, Lanzhou University, China

In MSD domain, the discrete wavelet transform (DWT) becomes one of the most popular methods since it has more advantages, such as localization and direction, as compared with pyramid based methods. Though DWT is an optimal tool for analyzing one dimensional (1D) piecewise smooth signal, it has limitations while expressing special characteristics effectively [12, 26].

Thus, new MSD methods are introduced in image fusion, such as Curvelet [18], Ridgelet [1], Contourlet, and Ripplet [14] etc, to overcome the limits of wavelet. Contourlet was proposed by M.N.Do and M.Vetterli. It provides different and flexible number of directions at each scale and can capture the intrinsic geometrical structure [5, 6], but Contourlet lacks shift-invariance property and causes pseudo-Gibbs phenomena around singularities since it needs downsampling and upsampling operations [2].

In order to get rid of the frequency aliasing of the Contourlet and enhance directional selectivity and shift-invariance, Cunha, Zhou, and M.N.Do proposed nonsubsampling contourlet transform (NSCT) [2]. Thus, in this paper NSCT is used as the MSD method.

Known as one of the third generation artificial neural networks, pulse coupled neural network (PCNN) is a visual cortex-inspired network characterized by the global coupling and pulse synchronization of neurons [10]. It has been observed that PCNN based image fusion methods outperform the conventional fusion methods [20, 21, 26].

However, Conventional PCNN model used for image fusion requires complex calculations. In order to improve the performance of image fusion methods based on traditional PCNN model, a series of modified and simplified PCNN models have been proposed. Spiking cortical model (SCM) is one of the simplified PCNN models that is deduced from primate visual cortex and mainly derived from Eckhorn's model, and has been proved an efficient image processing tool [27].

In recent years, researchers proposed several image fusion algorithms based on transform domain and PCNN, but most of these methods suffer from various problems. In [4] Deepika *et al.* proposed a combined method of multifocus image fusion and edge deduction based on NSCT and PCNN, but it suffers from the problems of unwanted image degradations. In [21] Wang, Z. *et al.* proposed a fast multifocus image fusion scheme based on a multi-channel PCNN (*m*-PCNN) model with easy extensibility capability, but also suffering from the problems of losing image fine details. Qu, X. *et al.* proposed an image fusion algorithm based on spatial frequency (SF) motivated PCNN in NSCT domain [22]. It works well for both multifocus image fusion and multi-source image fusion, but it uses same fusion rule for both high frequency coefficients and low frequency coefficients, which causes contrast reduction and loss of image details. The image fusion technique proposed by Xin, G. *et al.* based on dual-layer PCNN model with a negative feedback control mechanism in the NSCT domain has shown promising results in multifocus image fusion [23]. Literature [3] discussed fusion methods based on PCNN and NSCT in multimodal medical image fusion field. However, in most of these PCNN and NSCT based algorithms, the value of single pixel in spatial or MSD domain is used to motivate one neuron. In fact, humans are often sensitive to edges, directional features, etc. So, a pure use of single pixels is not enough. It is necessary to use spatial frequency, which stands for gradient energy in NSCT domain, to motivate SCM neurons [3, 22, 27].

In this paper, we propose an image fusion method by using the shift-invariance, multi-scale and multi-directional properties of NSCT along with human visual characteristics of SCM in such a way that can capture the subtle differences and fine details of source images, and finally result in fused images with high contrast and clarity.

2. Methods

2.1 Nonsubsamped contourlet transform (NSCT)

Contourlet is proposed by M.N.Do to obtain a sparse expansion for smooth contours, which overcomes the limitation of wavelet in representing contours by using square-shaped brush strokes and many fine "dots". Contourlet employs Laplacian pyramid (LP) for multi-scale decomposition, and the directional filter bank (DFB) for directional decomposition. The number of direction decomposition at each level can be different, which is much more flexible than the three directions in wavelet. Unfortunately, in the original contourlet, downsamplers and upsamplers are presented in both LP and DFB. Thus, it is not shift-invariant and causes pseudo-Gibbs phenomena around singularities. NSCT eliminates the downsamplers and upsamplers during the decomposition and reconstruction of image. Fig. 1(a) shows the decomposition framework of NSCT. Nonsubsamped pyramid filter bank (NSPFB) and nonsubsamped DFB (NSDFB) are used in NSCT. The NSPFB is achieved by using two-channel nonsubsamped 2-D filter banks. The NSDFB is achieved by switching off downsamplers and upsamplers in each two-channel filter bank in DFB tree structure and upsampling filters accordingly [2, 6].

The NSCT not only retains the features of Contourlet, but also has the properties of shift-invariance. When it is introduced into image fusion, sizes of different subbands are identical, which makes it easy to find the relationship among different subbands. This is beneficial for designing fusion rules.

The common NSCT-based image fusion approach consists of the following steps: Firstly, perform NSCT on source images to obtain lowpass subband coefficients and bandpass directional subband coefficients at each scale and each direction. Secondly, apply some fusion rules to select NSCT coefficients of the fused image. Finally, employ inverse NSCT to the selected coefficients and obtain the fused image. Fig. 2 shows the framework of NSCT-based fusion algorithm.

2.2 Spiking cortical model (SCM)

As one of the improved PCNN models, SCM can be used in image processing fields, such as image denoising, image segmentation, edge extraction, and image enhancement according to its robustness to geometrical changes. Two features of SCM make SCM itself more suitable for image processing. Firstly, it has been proved that SCM accords with Weber–Fechner law, for SCM has high sensitivity for low intensities of stimulus but low sensitivity for high intensities, and Weber–Fechner law describes human visual characteristics and is a logarithmic rule relating the level of subjective sense of intensity to the physical intensity of a stimulus. Secondly, time matrix of SCM can be recognized as human subjective sense of

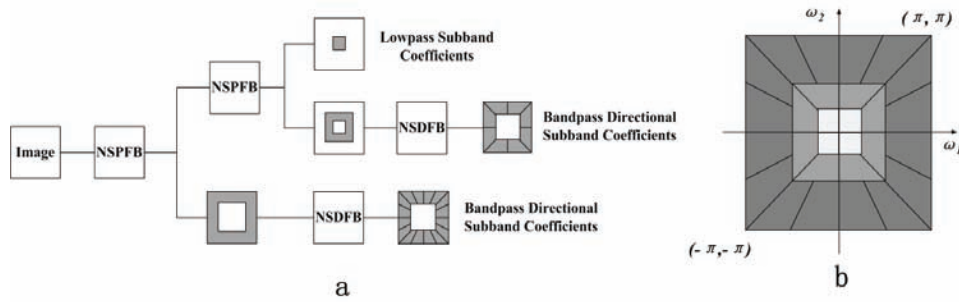


Fig. 1 *Nonsampled Contourlet transform: (a) decomposition framework and (b) idealized frequency partition.*

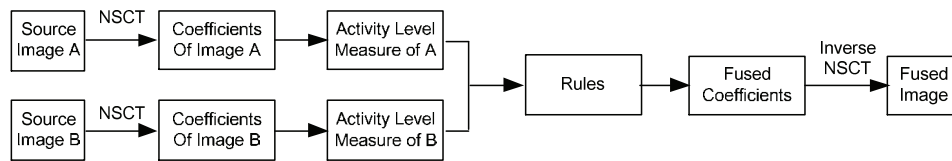


Fig. 2 *Schematic diagram of NSCT based fusion algorithm.*

stimulus intensity. Thus SCM can describe human visual perception better, and can achieve better effects in image processing field [27].

SCM is expressed as

$$U_{ij}(n) = fU_{ij}(n - 1) + S_{ij} \sum_{kl} W_{ijkl} Y_{kl}(n - 1) + S_{ij}, \tag{1}$$

$$E_{ij}(n) = gE_{ij}(n - 1) + hY_{ij}(n - 1), \tag{2}$$

$$Y_{ij}(n) = \begin{cases} 1, & 1/(1 + \exp(-\gamma(U_{ij}(n) - E_{ij}(n)))) > 0.5 \\ 0, & 1/(1 + \exp(-\gamma(U_{ij}(n) - E_{ij}(n)))) \leq 0.5 \end{cases}, \tag{3}$$

where $U_{ij}(n)$ is internal activity, S_{ij} is a stimulus, $Y_{ij}(n)$ is output, $E_{ij}(n)$ is dynamic threshold, W_{ijkl} is synaptic weight matrix applied to the linking field, f and g are decay constants, and h is threshold magnitude coefficient. As a typical neuronal nonlinear transform function, the Sigmoid function [9] is applied in SCM to improve performance, which helps make output reachable. γ is a parameter of Sigmoid function. The nonlinearity of Sigmoid function can be used to generate pulse. Sigmoid curve has an “S” shape, with its slope increasing as γ increases. From (1), (2) and (3), we can find there are 2 leaky integrators and 1 convolution item in SCM while the traditional PCNN functions include 3 leaky integrators and 2 convolution items. Thus SCM decreased computation complexity and is much less time consuming than PCNN. The advantage of SCM for image fusion not only lies in its human visual characteristics we mentioned above, but also lies in its light computation compared with PCNN [27].

The intersecting cortical model (ICM) proposed by Lindblad et al is a special case of PCNN when there are no linking neurons [7, 11, 15]. SCM will be ICM if linking strength of PCNN is set to zero. SCM possesses the advantages of both PCNN and ICM [27]. The SCM neuron model is shown in Fig. 3.

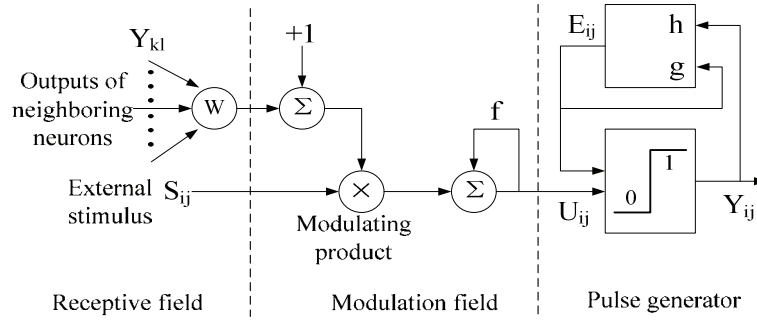


Fig. 3 SCM model.

2.3 Proposed image fusion scheme

PCNN was first used in contourlet domain for visible and infrared image fusion in literature [16], but the contourlet it applied is the original form and lacks shift-invariance, the PCNN it used is also the traditional form and needs complex computation. In addition, single coefficients is used to motivate PCNN directly. In fact, human vision system is often sensitive to features, e.g. edges. So, using value of single coefficient is not enough. In this paper, NSCT is used as the MSD method to provide a better representation of the contourlet, SCM is used as the simplified PCNN model to avoid heavy computation.

The notations used in this section are as follows: A, B, R represent two source images and final fused image, respectively. $C \in \{A, B, R\}$. LFS^C indicates the low frequency subband (LFS) of image C . $HFS_{g,h}^C$ indicates the high frequency subband (HFS) of image C at scale g and direction h . (i, j) denotes spatial location, thus $LFS^C(i, j)$, $HFS_{g,h}^C(i, j)$ denote coefficients located at (i, j) of low frequency and high frequency subband, respectively.

In NSCT, images can be decomposed into low frequency and high frequency subbands. The former determines gradation of light and the later relates with detail structure. They should be fused separately.

2.3.1 The fusion rule of low frequency coefficients

The coefficients in coarsest scale subband represent approximation component of source image. In most fusion applications, maximum selection rule (MSR) [13] was adopted to choose low frequency coefficients. According to this fusion rule, we select the low frequency coefficients of LFS^R from LFS^A or LFS^B . Here we define a new maximum selection rule as follow:

$$\text{LFS}^R(i, j) = \begin{cases} \text{LFS}^A(i, j), & |\text{LFS}^A(i, j)| - |\text{LFS}^B(i, j)| > \theta \\ \text{LFS}^A(i, j) \times 0.5 + \text{LFS}^B(i, j) \times 0.5, & \left| |\text{LFS}^A(i, j)| - |\text{LFS}^B(i, j)| \right| \leq \theta \\ \text{LFS}^B(i, j), & |\text{LFS}^B(i, j)| - |\text{LFS}^A(i, j)| > \theta \end{cases} \quad (4)$$

where threshold θ is an experimental value according to the resultant image. Threshold θ is defined as follow:

$$\theta = \frac{1}{2} \times \frac{\sum_{i=1}^M \sum_{j=1}^N (\text{LFS}^A(i, j) + \text{LFS}^B(i, j))}{M \times N}, \quad (5)$$

where M, N means image size.

2.3.2 The fusion rule of high frequency coefficients

The coefficients of HFS of source images are fused using SCM. As human vision system are sensitive to features such as edges, contours etc., so instead of using SCM in high frequency subbands directly, spatial frequency (SF) is considered as the gradient features of images to motivate SCM networks.

SF proposed by Eskicioglu et al. is calculated by row and column frequency [8]. It reflects the whole activity level of an image which means the larger the SF the higher the image resolution.

The SF is defined as

$$S_{i,j}^{g,h} = \sum_{i \in M, j \in N} (I_{i,j}^{g,h} - I_{i-1,j}^{g,h})^2 + (I_{i,j}^{g,h} - I_{i,j-1}^{g,h})^2, \quad (6)$$

where $S_{i,j}^{g,h}$ and $I_{i,j}^{g,h}$ denote the SF and the coefficients of the pixel that located at (i, j) on scale g and direction h , respectively.

SF in each high frequency subbands are inputted to SCM to motivate neurons and generate pulse of neurons as follow:

$$U_{i,j}^{g,h}(n) = fU_{i,j}^{g,h}(n-1) + S_{i,j}^{g,h} \sum_{k,l} W_{i,j,k,l}^{g,h} Y_{k,l}^{g,h}(n-1) + S_{i,j}^{g,h}, \quad (7)$$

$$E_{i,j}^{g,h}(n) = gE_{i,j}^{g,h}(n-1) + hY_{i,j}^{g,h}(n-1), \quad (8)$$

$$Y_{i,j}^{g,h}(n) = \begin{cases} 1, & 1 / \left(1 + \exp \left(-\gamma U_{i,j}^{g,h}(n) - E_{i,j}^{g,h}(n) \right) \right) > 0.5 \\ 0, & 1 / \left(1 + \exp \left(-\gamma U_{i,j}^{g,h}(n) - E_{i,j}^{g,h}(n) \right) \right) \leq 0.5 \end{cases}, \quad (9)$$

$$T_{i,j}^{g,h}(n) = T_{i,j}^{g,h}(n-1) + Y_{i,j}^{g,h}(n), \quad (10)$$

where $S_{i,j}^{g,h}$ is set as feeding input of SCM, $U_{i,j}^{g,h}(n)$ is internal activity, n denotes iteration times. If $Y_{i,j}^{g,h}(n)$ is equal to 1, it means the neuron will generate a pulse, or we can say one firing occurs. The sum of $Y_{i,j}^{g,h}$ in n iteration (namely the

firing times) is defined as $T_{i,j}^{g,h}(n)$ to represent the image information. Rather than $Y_{i,j}^{g,h}(n)$, researchers often analyze $T_{i,j}^{g,h}(n)$, because neighboring coefficients with similar features representing similar firing times in a given iteration times. In this paper, we set firing times $T_{i,j}^{g,h}(n)$ as criteria to select coefficients of high frequency subbands.

2.4 Fusion algorithm

Source images to be fused must be registered. The steps of the proposed image fusion algorithm are described briefly as follows:

- 1) Decompose source images A and B by NSCT to get low frequency and high frequency subbands coefficients of each image.
- 2) Select coefficients of LFS^R by using formula (4).
- 3) Calculate SF as described in formula (6) by using overlapping window on coefficients of HFS.
- 4) Input SF of each HFS into SCM to motivate the neural networks and generate pulse of neurons with formula (7) ~ (9). And then compute the firing times $T_{i,j}^{g,h}(n)$ by formula (10).
- 5) Fuse coefficients of each HFS by the following rules

$$HFS_{g,h}^R(i,j) = \begin{cases} HFS_{g,h}^A(i,j), & T_{i,j}^{g,h,A}(n) \geq T_{i,j}^{g,h,B}(n) \\ HFS_{g,h}^B(i,j), & T_{i,j}^{g,h,A}(n) < T_{i,j}^{g,h,B}(n) \end{cases} \quad (11)$$

- 6) Apply inverse NSCT on the fused LFS and HFS to get the final fused image.

The schematic diagram is shown in Fig. 4.

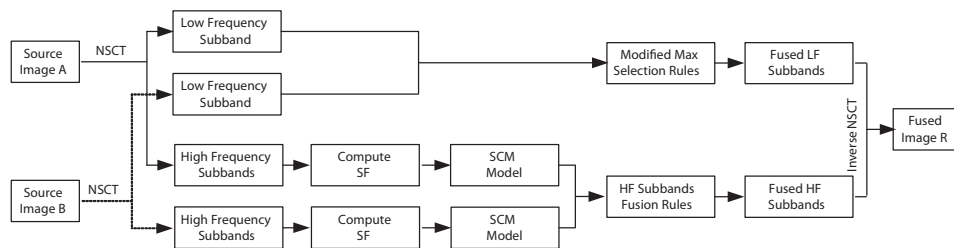


Fig. 4 Proposed fusion method.

3. Results

Our experiments are conducted by MATLAB R2007b on a PC with Intel Core (TM) 2 Duo T7500 2.2GHz. The decomposition parameter of NSCT is set as:

levels = [1, 2, 4], pyramid filter and directional filter are set as ‘pyrexc’ and ‘yk’, respectively.

In order to demonstrate effectiveness of the proposed fusion method, a large number of experiments have been conducted. After a number of tests, we set the parameters of SCM as follows: internal activity initialization is set to be 0’s and dynamic threshold initialization is set to be 1’s; f, g, h and γ are set to be 0.2, 0.9, 20, and 1, respectively; $k \times l = 3 \times 3$, the SCM is iterated 37 times, weight matrix of linking field W is given by (12)

$$W = \begin{pmatrix} 0.1091 & 0.1409 & 0.1091 \\ 0.1409 & 0 & 0.1409 \\ 0.1091 & 0.1409 & 0.1091 \end{pmatrix}. \tag{12}$$

We choose 4 evaluation criteria as objective analysis indices: mutual information (MI) [17], standard deviation (SD), energy of laplacian (EOL) and $Q^{AB/F}$ [24]. MI can be used to measure amount of information transferred from source images to final fused image. Fusion performance would be better and better with MI increasing. SD indicates deviation degree between grey values of pixels and the average one of the fused image. EOL is one of the useful indices to describe clarity of image. $Q^{AB/F}$ [24] is proposed by C.S.Xydeas et al. as an objective image fusion performance measure. The above 4 indices are mathematically described as

$$\begin{aligned} \text{MI} &= \frac{\sum_{i=0}^{L-1} \sum_{k=0}^{L-1} P_{A,R}(i, k) \log((P_{A,R}(i, k))/(P_A(i)P_R(k)))}{IE_A + IE_B} + \\ &+ \frac{\sum_{j=0}^{L-1} \sum_{k=0}^{L-1} P_{B,R}(j, k) \log((P_{B,R}(j, k))/(P_B(j)P_R(k)))}{IE_A + IE_B}, \end{aligned} \tag{13}$$

$$\text{SD} = \sqrt{\frac{1}{m \times n} \sum_{i=1}^m \sum_{j=1}^n (f(i, j) - \frac{1}{m \times n} \sum_{i=1}^m \sum_{j=1}^n f(i, j))^2}, \tag{14}$$

$$\begin{aligned} \text{EOL} &= \sum_{i=2}^{m-1} \sum_{j=2}^{n-1} (-f(i-1, j-1) - 4f(i-1, j) - f(i-1, j+1) - 4f(i, j-1) + \\ &+ 20f(i, j) - 4f(i, j+1) - f(i+1, j-1) - 4f(i+1, j) - f(i+1, j+1))^2, \end{aligned} \tag{15}$$

$$Q^{AB/F} = \frac{\sum_{n=1}^N \sum_{m=1}^M (Q^{AF}(n, m)\omega^A(n, m) + Q^{BF}(n, m)\omega^B(n, m))}{\sum_{n=1}^N \sum_{m=1}^M (\omega^A(n, m) + \omega^B(n, m))}, \tag{16}$$

where A and B are source images, R the final fused image, $m \times n$ the size of the image that has L grey levels; $f(i, j)$ denotes grey value of pixel (i, j) , $P(i)$ indicates probability of pixels whose grey value amount to i ; $P_{A,R}(i, k)$ and $P_{B,R}(i, k)$ are the normalized grey histogram between A and R and the normalized grey histogram

between B and R , respectively. IE_A and IE_B denote the information entropy (IE) of image A and B . $Q^{AF}(n, m) = Q_g^{AF}(n, m)Q_\alpha^{AF}(n, m)$. $Q_g^{AF}(n, m)$ and $Q_\alpha^{AF}(n, m)$ are the edge strength and orientation preservation values, respectively. $Q^{BF}(n, m)$ is similarly computed. $\omega^A(n, m)$ and $\omega^B(n, m)$ reflect the importance of $Q_g^{AF}(n, m)$ and $Q_\alpha^{AF}(n, m)$, respectively. The dynamic range of $Q^{AB/F}(n, m)$ is $[0, 1]$.

Fig. 5 shows three groups of source images: clock image group (A1, B1), logo image group (A2, B2), book image group (A3, B3). A1, B1 are focused on right and left, respectively. A2, B2 are focused on bottom half and upper half, respectively. A3, B3 are focused on background and foreground, respectively.

In order to prove the validity of the proposed fusion technique, several experiments are conducted. 5 other methods are adopted to compare with our proposed one (M6), which are Averaging method (M1), discrete wavelet transform (DWT) with DBSS (2, 2) (M2), Laplacian pyramid (M3), morphological pyramid (M4), PCA method (M5). Parameters of these methods are set by: pyramid level = 4, selection rules: high-pass = select max, lowpass = average [19].

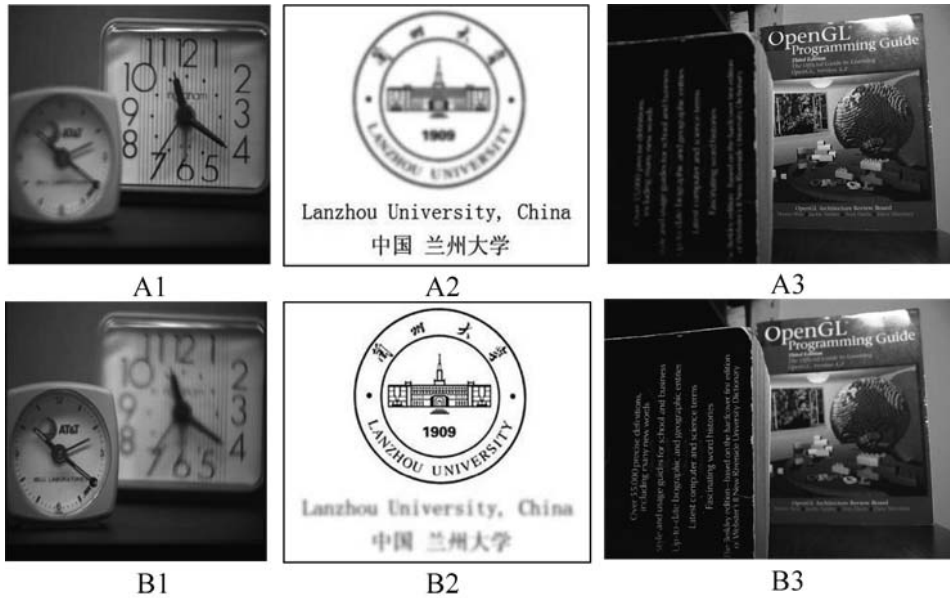


Fig. 5 Three groups of source images clock image group (A1, B1) logo image group (A2, B2) book image group (A3, B3) A1, B1, A3, B3 are all from website <http://www.imagefusion.org/>; A2, B2 are from our lab.

Fig. 6 and Fig. 7 show fusion results by using above mentioned 6 methods conducted on clock images and logo images. Fig. 8 and Fig. 9 show magnified details of different fusion results, respectively. In each figure, M_i ($i = 1, 2, \dots, 6$) indicates different fusion methods. For the comparison result of different methods conducted on book images, we only provide objective evaluation data in Section 4.2.

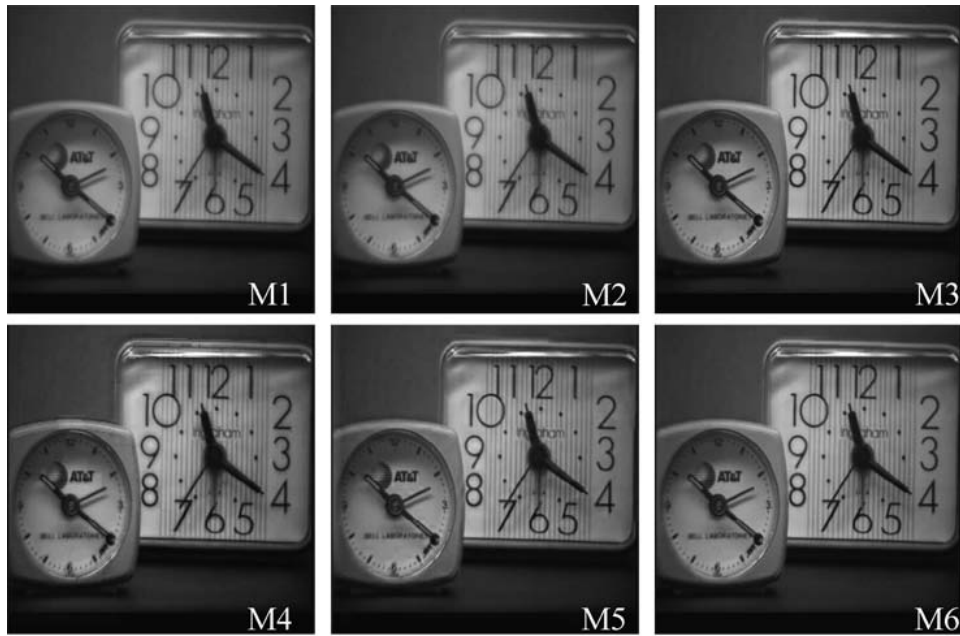


Fig. 6 Fusion results of different methods conducted on clock images: (M1) Averaging method; (M2) discrete wavelet transform (DWT) with DBSS (2, 2); (M3) Laplacian pyramid; (M4) morphological pyramid; (M5) PCA method; (M6) our method.



Fig. 7 Fusion results of different methods conducted on logo images.

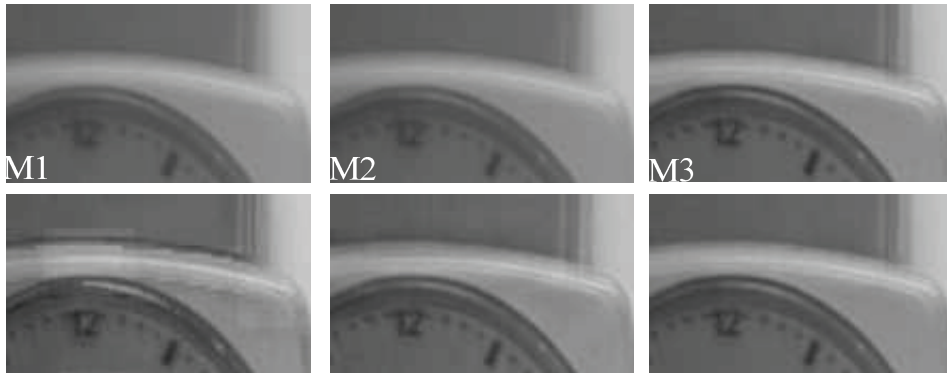


Fig. 8 Parts of the fused results of Fig. 6.

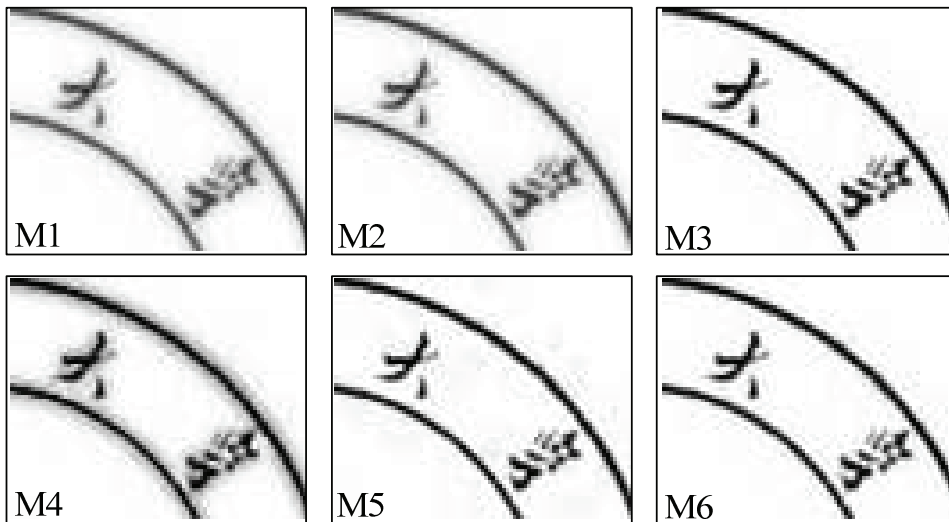


Fig. 9 Parts of the fused results of Fig. 7.

4. Discussion

4.1 Subjective evaluation and discussion

By carefully inspect the fused images obtained by 6 fusion methods in Fig. 6, Fig. 7, and the magnified details shown in Fig. 8 and Fig. 9, we can find that our proposed method possesses a satisfied visual effect compared to other 5 methods. In Fig. 6 ~ 9, M1 (Averaging method) as one of the easiest methods, eliminated too much image details and blurred the fused images (particularly see M1 of Fig. 9), M2 (discrete wavelet transform (DWT) with DBSS (2, 2)) produced noise around edges, margins and lines, which resulted in a kind of glow effect. In addition, we can see that Both M1 and M2 also reduced image contrast heavily. M4 (morphological

pyramid) suffered from the problem of blocking effect and contained unwanted image degradations in every source image group. M5 (PCA method) still brought in noised and fake dot information around outlines and contours, but not as much as M2 produced. As far as these six methods are concerned, the results of both M3 (Laplacian pyramid) and M6 (our proposed one) obtained better visual effects. Therefore, it is clear from the subjective visual evaluation that the proposed fusion method is effective in multifocus image fusion.

4.2 Objective evaluation and discussion

Tab. I and Fig. 10 report objective evaluations of the above-mentioned 6 methods. Experimental data shows that the differences of SD values of 6 fusion methods are slight and tiny. Thus we pay more attention to the other three evaluation indices. In the clock image group, the values of MI, EOL and QABF of our proposed M6 are the best. In the book image group, the values of MI and QABF of M6 are the best. Though in the book image group the EOL values of M6 is not as good as M4, it still outperformed the other 4 methods. In the logo image group, both MI and EOL of M6 get the highest values, the value of QABF of M6 get the second high value. From Fig. 10, it also can be seen that the evaluation results of Averaging method (M1) and PCA method (M5) are not as good as the other four ones.

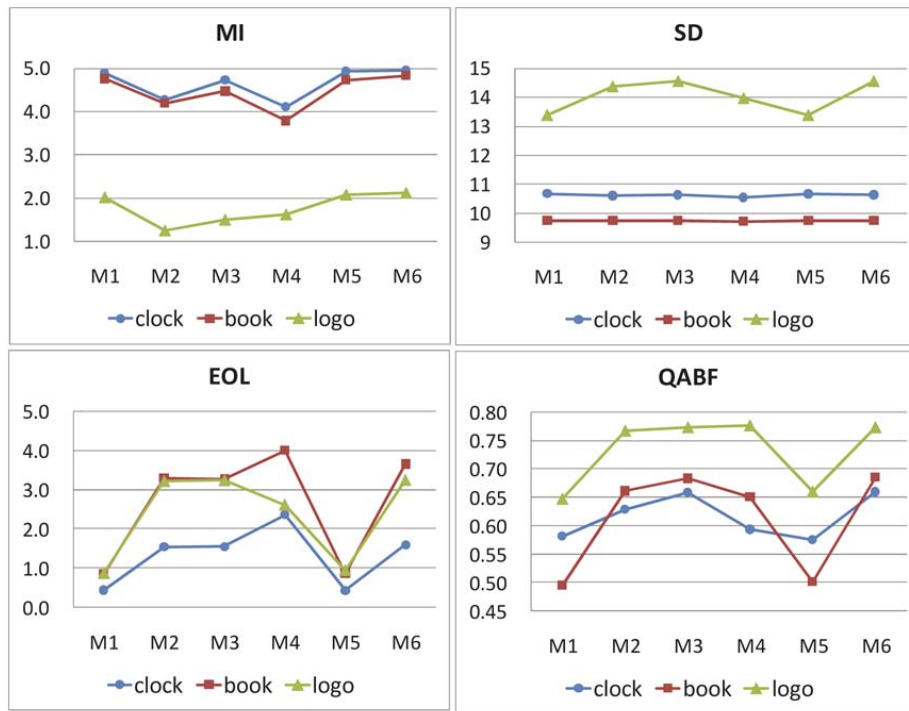


Fig. 10 Comparison of six fusion methods.

	Fused clock image				Fused book image				Fused logo image			
	MI	SD	EOL	QABF	MI	SD	EOL	QABF	MI	SD	EOL	QABF
M1	4.893	10.676	0.436	0.581	4.758	9.753	0.855	0.495	2.016	13.398	0.879	0.648
M2	4.275	10.598	1.538	0.629	4.182	9.756	3.293	0.661	1.254	14.364	3.227	0.767
M3	4.726	10.631	1.548	0.659	4.470	9.745	3.276	0.683	1.490	14.543	3.249	0.773
M4	4.112	10.540	2.354	0.593	3.784	9.725	3.996	0.651	1.626	13.972	2.624	0.777
M5	4.919	10.663	0.433	0.575	4.721	9.744	0.861	0.501	2.071	13.372	0.953	0.660
M6	4.959	10.626	1.590	0.659	4.828	9.744	3.644	0.686	2.122	14.543	3.253	0.774

Tab. I Comparison of six fusion method of three image groups.

	Noise1						Noise2						Noise3					
	MI	SD	EOL	QABF	MI	SD	EOL	QABF	MI	SD	EOL	QABF	MI	SD	EOL	QABF		
M1	3.577	10.683	0.560	0.364	M1	3.197	10.691	1.069	0.304	M1	2.954	10.638	1.573	0.271	0.238	0.271		
M2	2.779	10.642	1.818	0.347	M2	2.364	10.678	3.470	0.279	M2	2.108	10.615	5.118	0.238	0.238	0.238		
M3	2.913	10.622	1.776	0.358	M3	2.496	10.663	3.398	0.287	M3	2.244	10.692	5.012	0.246	0.246	0.246		
M4	2.856	10.521	1.591	0.355	M4	2.524	10.509	2.832	0.292	M4	2.309	10.523	4.043	0.253	0.253	0.253		
M5	3.575	10.668	0.561	0.361	M5	3.196	10.675	1.070	0.303	M5	2.952	10.691	1.574	0.270	0.270	0.270		
M6	2.952	10.689	1.541	0.336	M6	2.530	10.718	2.981	0.270	M6	2.269	10.734	4.397	0.234	0.234	0.234		

Tab. II Quantitative results of robustness test. The standard deviations of 3 different Gaussian noises Noise1, Noise2, Noise3 are set as $\delta_1 = 0.002$, $\delta_2 = 0.004$, $\delta_3 = 0.006$, respectively.

	Noise4				Noise5				
	MI	SD	EOL	QABF	MI	SD	EOL	QABF	
M1	2.765	10.646	2.071	0.247	M1	2.615	10.652	2.567	0.229
M2	1.925	10.623	6.712	0.214	M2	1.782	10.624	8.317	0.192
M3	2.059	10.634	6.611	0.220	M3	1.919	10.644	8.171	0.199
M4	2.167	10.559	5.216	0.228	M4	2.037	10.582	6.349	0.206
M5	2.765	10.627	2.072	0.248	M5	2.616	10.633	2.567	0.230
M6	2.076	10.660	5.811	0.211	M6	1.927	10.661	7.183	0.193

Tab. III Another group of quantitative results of robustness test. The standard deviations of 2 different Gaussian noises Noise4 and Noise5 are set as $\delta_4 = 0.008$ and $\delta_5 = 0.01$, respectively.

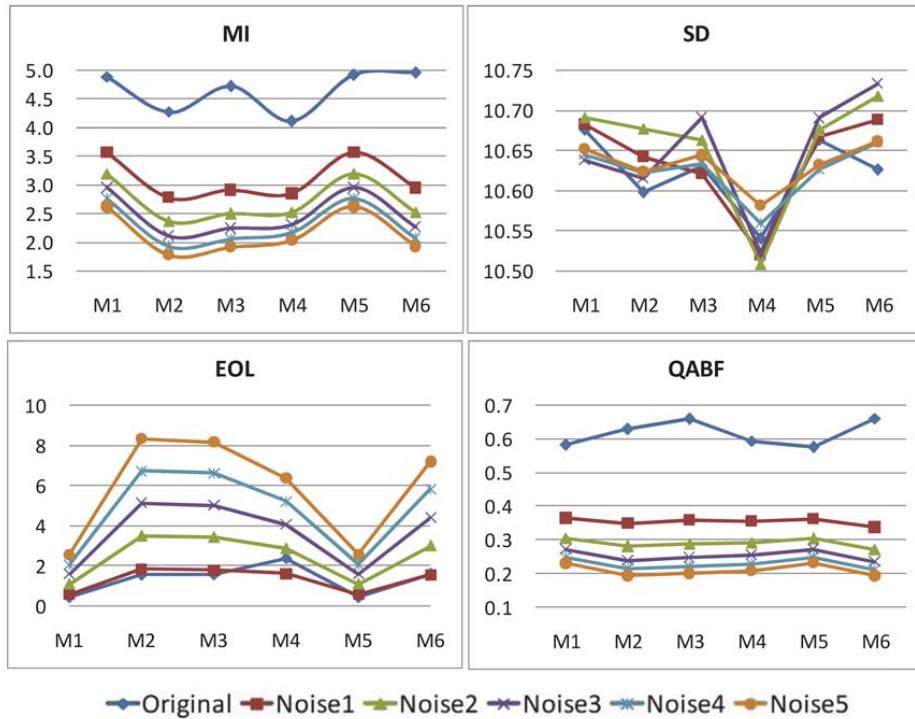


Fig. 11 Visual display of robustness test

4.3 Robustness evaluation of fusion methods

In order to evaluate the performance of the proposed method in a noisy environment, a series of robustness test experiments are conducted. Here we choose the two source clock images (A1 and B1 of Fig. 5) as robustness test images to illus-

trate experimental results. Firstly, we add five different Gaussian noises to the two source clock images and get five pair of noised source clock images. The Gaussian noises we implanted are namely Noise1, Noise2, Noise3, Noise4 and Noise5. The standard deviation of 5 noises are $\delta_1 = 0.002$, $\delta_2 = 0.004$, $\delta_3 = 0.006$, $\delta_4 = 0.008$ and $\delta_5 = 0.01$, respectively. Then the 6 fusion methods are applied to 5 groups of noised source images, and we get a new image dataset with 30 noisy fused image results. For these 5 groups of noisy fused images, we compare them to the corresponding original un-noised fused images (images in Fig. 6). Tab. II and Tab. III show experimental results of four evaluation indices. Fig. 11 clearly demonstrates the robustness comparison of different fusion methods under different noisy environments. From Tab. II, Tab. III and Fig. 11, we can see that 4 evaluation indices change regularly as noise changes, which proved that our proposed fusion method is also robust to Gaussian noises as the other 5 classic fusion methods do, and can be used in noised image environment.

The quantitative objective evaluation and comparison we discussed above verified that the proposed method is an effective fusion method of multifocus image both in noise-free and noisy environments.

5. Conclusions

NSCT is one of useful multiscale geometric analysis tools, which take full advantage of geometric regularity of image intrinsic structures. SCM is an improved PCNN model. It describes human visual perception better compared to traditional PCNN model. In this paper, we present a new multifocus image fusion scheme based on NSCT and SCM. The flexible multi-resolution, anisotropy, and directional expansion characteristics of NSCT are associated with global coupling and pulse synchronization features of SCM. Experimental comparisons conducted on different fusion methods prove the effectiveness of the proposed fusion method. Robustness test experiments verify that our method can be used in noisy image processing field.

Acknowledgement

The authors would like to thank the anonymous reviewers and editors for their invaluable suggestions. This work was jointly supported by the National Natural Science Foundation of China (No. 61375029, No. 61162021, No. 61175012), and the Fundamental Research Funds for the Central Universities (No. 31920140086); This work was also supported by the Talent Introduction Project of Northwest University for Nationalities (No. xbmuyjrc201504).

References

- [1] CANDES E.J. *Ridgelets: theory and applications*. Stanford University, 1998. PhD thesis, Stanford University.
- [2] DA CUNHA A.L., ZHOU J., DO M.N. The nonsubsampling contourlet transform: theory, design, and applications. *IEEE Transactions on Image Processing*. 2006, 15(10), pp. 3089–3101, doi: 10.1109/tip.2006.877507.

- [3] DAS S., KUNDU M.K. NSCT-based multimodal medical image fusion using pulse-coupled neural network and modified spatial frequency. *Medical & biological engineering & computing*. 2012, 50(10), pp.1105–1114, doi: 10.1007/s11517-012-0943-3.
- [4] DEEPIKA M.M., VAITHYANATHAN V. An efficient method to improve the spatial property of medical images. *Journal of Theoretical and Applied Information Technology*. 2012, 35(2), pp. 141–148. Available from: <http://www.jatit.org/volumes/Vol135No2/2Vol135No2.pdf>.
- [5] DO M.N., VETTERLI M. Framing pyramids. *IEEE Transactions on Signal Processing*. 2003, 51(9), pp. 2329–2342, doi: 10.1109/tsp.2003.815389.
- [6] DO M.N., VETTERLI M. The contourlet transform: an efficient directional multiresolution image representation. *IEEE Transactions on Image Processing*. 2005, 14(12), pp. 2091–2106, doi: 10.1109/tip.2005.859376.
- [7] EKBLAD U., KINSER J.M., ATMER J. The intersecting cortical model in image processing. *Nuclear Instruments and Methods in Physics Research Section A: Accelerators, Spectrometers, Detectors and Associated Equipment*. 2004, 525(1), pp. 392–396, doi: 10.1016/j.nima.2004.03.102.
- [8] ESKICIOGLU A.M., FISHER P.S. Image quality measures and their performance. *IEEE Transactions on Communications*. 1995, 43(12), pp. 2959–2965, doi: 10.1109/26.477498.
- [9] FORGAC R., MOKRIS I. Feature generation improving by optimized PCNN. In: *Proceedings of the 6th International Symposium on Applied Machine Intelligence and Informatics*, Herl'any, Slovakia. IEEE, 2008, pp. 203–207, doi: 10.1109/sami.2008.4469166.
- [10] JOHNSON J L, PADGETT M L. PCNN models and applications. *IEEE transactions on neural networks*. 1998, 10(3), pp. 480–498, doi: 10.1109/72.761706.
- [11] KINSER J.M. Simplified pulse-coupled neural network. In: *Proceedings of Applications and Science of Artificial Neural Networks II (SPIE 2760)*, Orlando, Florida, USA. The International Society for Optical Engineering, 1996, pp. 563–567, doi: 10.1117/12.235951.
- [12] LE PENNEC E., MALLAT S. Sparse geometric image representations with bandelets. *IEEE Transactions on Image Processing*. 2005, 14(4), pp. 423–438, doi: 10.1109/tip.2005.843753.
- [13] LI H., MANJUNATH B S., MITRA S.K. Multisensor image fusion using the wavelet transform. *Graphical models and image processing*. 1995, 57(3), pp. 235-245, doi: 10.1006/gmip.1995.1022.
- [14] LI S., YANG B., HU J. Performance comparison of different multi-resolution transforms for image fusion. *Information Fusion*. 2011, 12(2), pp. 74–84, doi: 10.1016/j.inffus.2010.03.002.
- [15] LINDBLAD T., KINSER J.M., LINDBLAD T. Image processing using pulse-coupled neural networks. Heidelberg: Springer, 1998, doi: 10.1007/978-1-4471-3617-0.
- [16] LIU S., FANG Y. Infrared image fusion algorithm based on contourlet transform and improved pulse coupled neural network. *Journal of Infrared and Millimeter Waves (Chinese Edition)*. 2007, 26(3), pp. 217. Available from: http://en.cnki.com.cn/Article_en/CJFDTOTAL-HWYH200703013.htm.
- [17] QU G., ZHANG D., YAN P. Information measure for performance of image fusion. *Electronics letters*. 2002, 38(7), pp. 313–315, doi: 10.1049/el:20020212.
- [18] STARCK J.L., CANDÈS E.J., DONOHO D.L. The curvelet transform for image denoising. *IEEE Transactions on Image Processing*. 2002, 11(6), pp. 670–684, doi: 10.1109/icip.2001.958937.
- [19] WANG Z., MA Y., CHENG F. Review of pulse-coupled neural networks. *Image and Vision Computing*. 2010, 28(1), pp. 5–13, doi: 10.1016/j.imavis.2009.06.007.
- [20] WANG Z., MA Y., GU J. Multi-focus image fusion using PCNN. *Pattern Recognition*. 2010, 43(6), pp. 2003–2016, doi: 10.1016/j.patcog.2010.01.011.
- [21] WANG Z., MA Y. Medical image fusion using m-PCNN. *Information Fusion*. 2008, 9(2), pp. 176–185, doi: 10.1016/j.inffus.2007.04.003.

- [22] XIAO-BO Q., JING-WEN Y., HONG-ZHI X. Image fusion algorithm based on spatial frequency-motivated pulse coupled neural networks in nonsubsamped contourlet transform domain. *Acta Automatica Sinica*. 2008, 34(12), pp.1508–1514, doi: 10.3724/sp.j.1004.2008.01508.
- [23] XIN G., ZOU B., LI J., LIANG Y. Multi-focus image fusion based on the nonsubsamped contourlet transform and dual-layer PCNN model. *Information Technology Journal*. 2011, 10(6), pp. 1138–1149, doi: 10.3923/itj.2011.1138.1149.
- [24] XYDEAS C.S., PETROVIĆ V. Objective image fusion performance measure. *Electronics Letters*. 2000, 36(4), pp. 308–309, doi: 10.1049/el:20000267.
- [25] YANG S., WANG M., LU Y.X. Fusion of multiparametric SAR images based on SW-nonsubsamped contourlet and PCNN. *Signal Processing*. 2009, 89(12), pp. 2596–2608, doi: 10.1016/j.sigpro.2009.04.027.
- [26] YONG Y., DONGSUN P., SHUYING H. Medical image fusion via an effective wavelet-based approach. *EURASIP Journal on Advances in Signal Processing*. 2010, 2010(1): 579341, pp. 13, doi: 10.1155/2010/579341.
- [27] ZHAN K., ZHANG H., MA Y. New spiking cortical model for invariant texture retrieval and image processing. *IEEE Transactions on Neural Networks*. 2009, 20(12), pp. 1980–1986, doi: 10.1109/tnn.2009.2030585.
- [28] ZHANG Z., BLUM R.S. A categorization of multiscale-decomposition-based image fusion schemes with a performance study for a digital camera application. *Proceedings of the IEEE*. 1999, 87(8), pp. 1315–1326, doi: 10.1109/5.775414.